SF2A 2021
A. Siebert, K. Baillié, E. Lagadec, N. Lagarde, J. Malzac, J.-B. Marquette, M. N'Diaye, J. Richard, O. Venot (eds)

THE IMPACT OF SURFACE FLOWS AT DIFFERENT SCALES: EXOPLANET DETECTABILITY IN RADIAL VELOCITY AND HIGH-PRECISION ASTROMETRY

N. Meunier[1] and A.-M. Lagrange[1, 2]

Abstract. It is now well accepted that stellar activity prevents the detection of Earth-like planets around solar type stars when using the radial velocity technique. Although the impact of dark spots and bright plages, through various processes, is now well modelled, surface flows at different time scales (granulation, supergranulation, meridional circulation) also lead to important radial velocity signatures due to their temporal variability but have been less studied. Those signatures are larger than an Earth-like signal. In this talk, we will focus on those flows, which we have studied based on our knowledge of the Sun and extended towards other stars. We will also show that a high-precision astrometric mission would not be strongly impacted by stellar activity for such planets.

Keywords: Stellar activity - Solar-type stars - Exoplanets - Convection - Radial velocity - Astrometry

1 Introduction

A large variety of stellar processes affects radial velocity (hereafter RV) temporal variations (see Meunier 2021, for a review). The best studied impact is due to the contrast of spots and plages, distorting the shape of the spectral lines as structures rotate (Saar & Donahue 1997). Another major effect is due to the inhibition of the convective blueshift in plages, which appears to be dominant for a star like the Sun (Lagrange et al. 2010; Meunier et al. 2010): this affects both short timescales (rotation) and long timescales (cycles). Surface flows at different scales also directly impact radial velocities. Granulation (and, at a larger scale, supergranulation) produces stochastic variabilities, following a specific power law with a plateau a long periods (Harvey 1984; Meunier et al. 2015), while pulsations mostly affect very short periods. Finally, meridional circulation is a large scale flow, mostly poleward in the solar case, but not yet observable for other stars, which also affects radial velocities if variable with time (Makarov 2010; Meunier & Lagrange 2020a). The inhibition of the convection leads to RV amplitudes up to a few m/s. The other aforementioned effects lead to RV variations with amplitudes typically in the 0.4-1 m/s range for old main-sequence FGK stars. They produce a barrier at the $\sim$1 m/s level. This is to be compared with the Earth signal, below 10 cm/s. Conversely, there are many less processes contributing to the stellar astrometric signal, which should not prevent to detect low mass planets if high precision can be reached (Lagrange et al. 2011).

2 Our approach

Our approach is twofold. First, we used our extensive knowledge of the Sun to better understand these different processes. We therefore developed reconstruction of the integrated signal based on solar observations (including with spatial resolution of the structures at the surface Lagrange et al. 2010; Meunier et al. 2010), then built a model validated in the solar case (Borgniet et al. 2015). This model was then extrapolated to other stars (Meunier et al. 2019). This allowed us to produce a very large amount of synthetic time series of radial velocities for FGK main old sequence stars, but also in photometry (Meunier & Lagrange 2019b), astrometry (Meunier et al. 2020) and chromospheric emission ($\log R'_{HK}$). This approach is complementary to others, such as RV

[1] Univ. Grenoble Alpes, CNRS, IPAG, F-38000 Grenoble, France
[2] LESIA, Observatoire de Paris, Université PSL, CNRS, Sorbonne Université, Univ. Paris Diderot, Sorbonne Paris Cité, 5 place Jules Janssen, 92195 Meudon, Franc

observations of the Sun as a star with HARPS-N (e.g. Collier Cameron et al. 2019), coordinated campaigns (Lopez et al. 2019), or more simple simulations (e.g. Desort et al. 2007; Dumusque et al. 2014).

Our simulations primarily include the contributions of spots and plages, and the inhibition of the convective blueshift (Meunier et al. 2019). We generated structures with a realistic spatio-temporal distribution, size and lifetime distributions and contrasts. Structures of different types are generated in a coherent way. The parameters cover F6-K4 stars with moderate activity level (young active stars are excluded at this stage because their parameters are less well constrained and different from the solar case). A second type of simulations takes pulsations, granulation and supergranulation into account. We performed a first simulation based on the proper number of granules and supergranules to check Harvey's law (Meunier et al. 2015), and later generated a large amount of time series based on their expected power law (Meunier & Lagrange 2019c, 2020b). The amplitude of the granular signal was scaled to the solar one with two different assumptions (low and high), with a dependence on spectral type. Supergranulation amplitude is also scaled to granulation. As for meridional circulation, we have so far only reconstructed the temporal variability in the solar case, based on the observations of Ulrich (2010), and extrapolated the amplitudes to other stars following numerical simulation prescriptions (Brun et al. 2017). Full synthetic simulations remain to be built.

We present here examples illustrating four important objectives on our approach: 1/ Predict the expected RV amplitudes for the different contributions; 2/ Understand correction method limitations; 3/ Quantify the impact on exoplanet mass characterisation, for example when performing an RV follow-up of transit detections, and compare them with high-precision astrometry; 4/ Quantify the impact on exoplanet detectability in RV, and compare them with high-precision astrometry.

3 Results

3.1 Predicting the expect RV amplitudes for the different contributions

The typical amplitude of magnetic activity (spots, plages, inhibition of the convective blueshift) is strongly dependent on the activity of the stars (average level and variability), with a rms (root-mean-square) RV between a few 0.1 m/s and several m/s (Meunier & Lagrange 2019a). Stellar inclination also impacts the amplitude. Simulations of granulation (Meunier et al. 2015) led to a solar rms of 0.8 m/s, a value larger than the observed one (0.4 m/s, Pallé et al. 1999), or from HD simulations (Sulis et al. 2020). The difference could be due some center-to-disk effects, or the use of a single spectral line in observations. The amplitude decreases from F to K stars. The supergranular signal shows variation with an rms between 0.3 and 1.2 m/s, in agreement with the solar observations of Pallé et al. (1999) in a single spectral line (0.7 m/s). The amplitude is expected to decrease from F to K stars, like granulation. Finally, our solar reconstruction of the large scale meridional circulation provided an amplitude in the 1-2 m/s range (Meunier & Lagrange 2020a). The variability is the highest for a star seen pole-on, and the sign of the variability reverses for a latitude around 30°, leading to a still important variability for a star seen edge-on. There may be a relation of the meridional circulation with the solar cycle, but possibly shifted in phase. Our extrapolation to FGK stars gave amplitudes in the 0.1-4 m/s range.

3.2 Understanding method limitations when correcting for stellar activity in RV

Many methods have been used to attempt to correct for the stellar contribution to RV variations, to be able to extract planetary signals. Some of them are based on proxy of stellar activity such as the $\log R'_{HK}$ indicator. A linear correlation between the two observables is often used, although it has been known to leave residuals: this correlation arises from the fact that both the inhibition of the convective blueshift in plages and the chromospheric emission are related to the same structures. The study of the synthetic time series (Meunier et al. 2019) allowed us to identify an effect leading to a non-linearity between RV and $\log R'_{HK}$, as the relationship is different between the ascending and descending phases of the cycles. This is due to the combination of two effects: due to the butterfly diagram of activity pattern, structures are on average at different distances from disk center during the cycle, while the chromospheric emission and the convective blueshift inhibition both depend on the position on the disk, but with different projection effects. We proposed a simple way to take this into account, by modeling the RV variability using a function of $\log R'_{HK}$ and of the phase of the cycle (providing an estimate of a cycle period can be made). We found that the rms of the residual could in such a case be indeed significantly improved with respect to the linear correction for some configurations. Some additional residuals remain, more stochastic, because at any given time, there is a dispersion in latitude of

the plages. We conclude that this should degrade the detectability in RV. Transit detection with further mass characterisation in RV may be easier, as discussed in the next section.

3.3 Quantifying the impact on exoplanet mass characterisation in transit follow-up

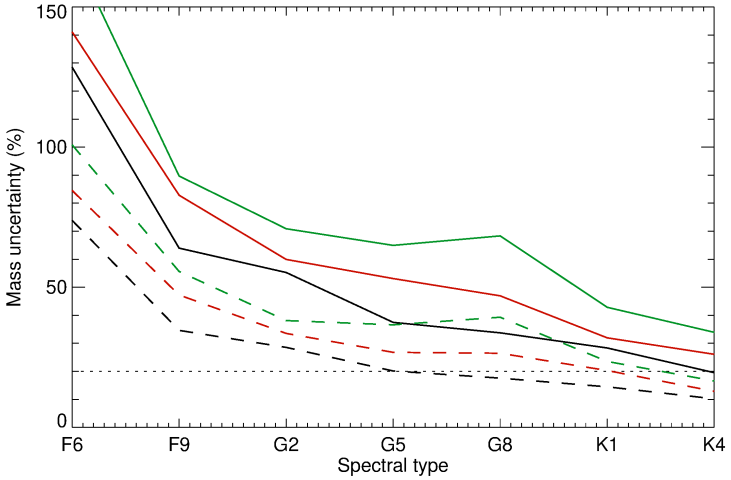

Fig. 1. Mass uncertainty for 1 M_{Earth} (solid) and 2 M_{Earth} (dashed), in the inner part of the habitable zone (black), middle (red) and outer part (green) versus spectral type, for a low level of granulation, supergranulation (both averaged over 1 h), spot, plages, and convective blueshift inhibition.

We used these synthetic time series to test the uncertainty on the mass estimation in a transit follow up. We focused on Earth-like planets in the habitable zone around solar-type stars, with masses of typically 1-2 M_{Earth}. The signal of the planet is first added to the synthetic stellar signal. We then assumed that the transit provides a precise estimate of the period and phase of the planet, and finally fitted the mass. The rms of the fitted mass on all realisations provided an estimate of the expected uncertainty on the mass. When considering the contributions due to pulsations, granulation, and supergranulation (Meunier & Lagrange 2020b), assuming 1-hour exposure time, we found that even with a very large amount of nights (>1000 over 10 years), the uncertainty for 1 M_{Earth} is above the 20% expected for PLATO, except for the lowest assumption for the stellar signal and K stars. The performance was slightly better for 2 M_{Earth}. The same computation made for the magnetic activity shows a worse performance, and again the uncertainty is always above 20%, as shown in Fig. 1. For the solar case and 1 M_{Earth} for example, the uncertainty is a factor 2 above 20%. By comparison, a high-precision astrometric mission with the performance of The Theia Collaboration et al. (2017) would allow to reach uncertainties of 20% or better (down to 10%) for a star at 10 pc, 1-2 M_{Earth} in the habitable zone, assuming 50 visits over 3.5 y and a noise of 0.2 μarcsec per measurement (Meunier et al. 2020).

3.4 Quantifying the impact on exoplanet detectability

We first estimated the mass of the detectable planet using a very simple analysis of the rms RV derived from these simulations and a threshold based on the performance of the best methods in the blind test performed in Dumusque et al. (2017). This showed that it was not possible to reach Earth mass planets in the habitable zone around solar-type stars (Meunier & Lagrange 2019a). To move further, a systematic analysis similar to that of Sect. 3.2 can be applied to detectability. Instead of assuming the period and phase of the planet found using its transits, a false alarm probability is computed on the time series, and peaks above this level in the periodogramme are considered to be detections. These detections are compared with the true parameters of the planet added to the stellar signal, which allows to estimate detection rates and false positive rates. Such blind tests on the pulsation-granulation-supergranulation time series, again with 1-hour exposure time, showed that the level of detection rates is low, typically 20% for G2 stars and 1266 nights over 10 years. Furthermore, there is a large amount of false positives, well above the 1% level. The signal is then dominated by supergranulation. The same blind tests made when considering the magnetic activity contribution (spots, plages, inhibition of

the convective blueshift in plages) leads to worse performance (with a correction as in Sect. 3.2): preliminary results for G2 stars and 1 M_{Earth} show a detection rate around 2% only, and more than 60% false positives, most of them at low periods however. The false positive rate in the habitable zone is of the order of 2-5%. By comparison, the detection rates for astrometry, again based on the The Theia Collaboration et al. (2017) configuration, leads to very good detection rates: only 10 to 20% of the planets are missed. The level of false positive in the habitable zone is below 0.1% (Meunier et al. 2020).

4 Conclusion and perspectives

We conducted a very fruitful approach, based on complex and realistic synthetic time series and a systematic analysis of these time series. For the first time, many processes were taken into account. The detectability of long-period exoplanets is affected by all processes, in which surface flows play an crucial role. Blind tests show that the mass characterisation in transit follow-up is poor for FGK stars and Earth mass planets in the habitable zone, and their detectability with RV alone is low (including a high level of false positive). The performance is much better for high-precision astrometry, although the technical challenges of such a mission is still problematic. Future work will focus on combining all processes and on improving the RV simulations to provide more observables, in order to test more correction methods. It will indeed be necessary to improve correction techniques based on the knowledge of the physical processes to be able to control the residuals and reach lower mass planets.

References

Borgniet, S., Meunier, N., & Lagrange, A.-M. 2015, A&A, 581, A133

Brun, A. S., Strugarek, A., Varela, J., et al. 2017, Astrophys. J., 836, 192

Collier Cameron, A., Mortier, A., Phillips, D., et al. 2019, MNRAS, 487, 1082

Desort, M., Lagrange, A. M., Galland, F., Udry, S., & Mayor, M. 2007, A&A, 473, 983

Dumusque, X., Boisse, I., & Santos, N. C. 2014, ApJ, 796, 132

Dumusque, X., Borsa, F., Damasso, M., et al. 2017, A&A, 598, A133

Harvey, J. W. 1984, in Probing the depths of a Star: the study of Solar oscillation from space, ed. R. W. Noyes, & E. J. Rhodes Jr., JPL, 400, 327

Lagrange, A.-M., Desort, M., & Meunier, N. 2010, A&A, 512, A38

Lagrange, A.-M., Meunier, N., Desort, M., & Malbet, F. 2011, A&A, 528, L9

Lopez, T. A., Barros, S. C. C., Santerne, A., et al. 2019, A&A, 631, A90

Makarov, V. V. 2010, Astrophys. J., 715, 500

Meunier, N. 2021, arXiv e-prints, arXiv:2104.06072

Meunier, N., Desort, M., & Lagrange, A.-M. 2010, A&A, 512, A39

Meunier, N. & Lagrange, A. M. 2019a, A&A, 628, A125

Meunier, N. & Lagrange, A. M. 2019b, A&A, 629, A42

Meunier, N. & Lagrange, A. M. 2019c, A&A, 625, L6

Meunier, N. & Lagrange, A. M. 2020a, A & A, 638, A54

Meunier, N. & Lagrange, A. M. 2020b, A & A, 642, A157

Meunier, N., Lagrange, A. M., & Borgniet, S. 2020, A & A, 644, A77

Meunier, N., Lagrange, A.-M., Borgniet, S., & Rieutord, M. 2015, A&A, 583, A118

Meunier, N., Lagrange, A. M., Boulet, T., & Borgniet, S. 2019, A&A, 627, A56

Meunier, N., Lagrange, A.-M., & Cuzacq, S. 2019, A&A, 632, A81

Pallé, P. L., Roca Cortés, T., Jiménez, A., GOLF Team, & Virgo Team. 1999, in Astronomical Society of the Pacific Conference Series, Vol. 173, Stellar Structure: Theory and Test of Connective Energy Transport, ed. A. Gimenez, E. F. Guinan, & B. Montesinos, 297

Saar, S. H. & Donahue, R. A. 1997, Astrophys. J., 485, 319

Sulis, S., Mary, D., & Bigot, L. 2020, A&A, 635, A146

The Theia Collaboration, Boehm, C., Krone-Martins, A., et al. 2017, arXiv:1707.01348

Ulrich, R. K. 2010, Astrophys. J., 725, 658